Available online at www.sciencedirect.com

ScienceDirect

Physics Procedia 12 (2011) 7–15

Physics Procedia

LiM 2011

Towards Friction Control using laser-induced periodic Surface Structures

J. Eichstädt*, G.R.B.E. Römer, A.J. Huis in't Veld

University of Twente, Chair of Applied Laser Technology, P.O. Box 217, Enschede 7500 AE, The Netherlands

Abstract

This paper aims at contributing to the study of laser-induced periodic surface structures (LIPSS) and the description of their tribological properties in order to facilitate the knowledge for contact mechanical applications. To obtain laser parameters for LIPSS formation, we propose to execute two D2-Experiments. For the transfer of results from static experiments to areas of LIPSS we propose the discrete accumulation of fluences. Areas covered by homogeneously distributed LIPSS were machined. Friction force of these areas was measured using a tribometer in a ball on flat configuration. The friction force was found to be higher on the structured area than on the initial surface.

Keywords: Laser Surface Texturing; Laser-induced periodic surface structures; Nanostructures; Tribology; Friction; High precision contact mechanics; Wafer chucks

1. Introduction

High Precision Contact Mechanics (HPCM), such as wafer chucks, are important for the position accuracy of a wafer on a chuck [1]. To control the position accuracy, the control of friction properties is required. A Method to control this type of surface functions could be laser-induced periodic surface structures (LIPSS). The use of LIPSS needs first the transfer of existing knowledge to a systematic extended area structuring and secondly the determination of their mechanical properties.

Commonly two methods are applied for structuring areas covered with LIPSS, mask projection [2-3] and direct writing [4-7]. Machining structures, requires information about parameter such as pulse energy E_P [J], pulse repetition frequency f_R [Hz], focused beam radius ω_0 [m], defined as $1/e^2$-radius, pulse distance s [m], scanning speed v [m/s] and number of overscans N_{OS} [-]. Usually experiments to determine these parameters are executed in a empirical way.

The use of LIPSS, as a tool to influence tribological properties, was already proposed in 1999 by Yu and Lu for the reduction of stiction problems of hard disk drives [3]. The influence of femtosecond (fs) initiated LIPSS was investigated by Mizuno et al. [4] and was found in the reduction of lateral as well as decrease of adhesive force.

* Corresponding author. Tel.: +31 53 489 2434.
E-mail address: j.eichstadt@utwente.nl.

doi:10.1016/j.phpro.2011.03.099

Another study reports a decrease of friction for full and increase for partially structured areas [6]. These results, mainly obtained on DLC coatings with fs pulses, provide only limited information about the influence of LIPSS on tribological properties.

In order to obtain laser parameter for LIPSS we propose to execute two D^2-Experiments [8]. For the transfer of results obtained in static experiments to areas of LIPSS we propose to calculate the discrete accumulation of fluences Φ [J/cm^2]. Analysis of geometrical dimensions and dynamic friction properties complete this investigation.

2. Theory

LIPSS generated by Gaussian fs pulses are observed for multi pulse irradiation and within a range of Φ between laser-induced modification and ablation [9]. LIPSS are confined in annular surface regions of inner diameter D_I [m] and outer D_O [m] [10]. Regarding these experimental observations, it seems to be possible to determine the local fluence Φ and the number of pulses per location N_P [-] of LIPSS, for an unknown laser-material combination, by conducting two D^2-Experiments: I) Single pulse experiment to identify a range of Φ, using the threshold fluence Φ_{th} for modification and ablation and II) Multi pulse experiment within the range to identify Φ_{LIPSS} and N_P for LIPSS.

Analysis of the surface after irradiation, reveal different morphologies dependent on the local fluence,

$$\Phi(x,y) = \int_{-\infty}^{\infty} I(x,y,t)dt\,, \tag{1}$$

where *(x, y)* [m] are Cartesian coordinates, t [s] is time and I [W/m^2] intensity. The threshold fluence, of these morphologies, can be determined by measuring E_P and D_O of the optically induced modification [8]

$$D_O^2 = 2\omega_0^2 \cdot \ln\left(\frac{\Phi_0}{\Phi_{th}}\right). \tag{2}$$

The peak fluence $\Phi_0 = 2E_P/(\pi\,\omega_0^2)$ can be derived by spatial integration

$$E_P = \int_{-\infty}^{\infty}\int_{-\infty}^{\infty} \Phi(x,y)dxdy\,. \tag{3}$$

Replacing in equation *(2)* fluence by energy gives a linear relation between D^2 and $ln(E_P)$. The threshold values can change, dependent on N_P, referred to as incubation, for which a power law $\Phi_{th}(N_P) = \Phi_{th}(1) * N_P^{\xi-1}$ has been found [11]. $\Phi_{th}(N_P)$ is the threshold fluence for N_P pulses per location, ξ [-] is a material dependent coefficient, referred to as incubation factor. Assuming LIPSS are observed within the second D^2-Experiment, Φ_{LIPSS} can be determined by measuring D_O of the LIPSS region.

The parameter Φ_{LIPSS} and N_P, obtained by placing pulses statically, on one location, needs to be transferred to parameter for machining areas dynamically. For scanning areas, pulses are placed with a discrete distance s to each other on the surface. The time T [s] between subsequent pulses, of a constant frequency f_R pulsed laser source, is used to move the beam, with a speed v from one position to another. If $s < 2\omega_0$ irradiated areas overlapping. In this experiment overlap is defined as $(\varphi) = 1-(v/(f_R 2\omega_0))$. Machining areas dynamically has two consequences: 1) Each previous and subsequent pulse contributes, two dimensional, with a part of its E_P to an area. 2) For each location within the irradiated area the fluence applied by subsequent pulses is different. To obtain similar results both statically

$$\Phi_{SA}(x,y) = \Phi_{LIPSS} \cdot N_P \cdot e^{-2\frac{x^2+y^2}{\omega_0^2}}, \tag{4}$$

and dynamically, not only the number of pulses per location but rather the accumulation of fluence has to be taken into account,

$$\Phi_{DA}(x,y) = \Phi_{LIPSS} \cdot N_{OS} \cdot \sum_m \sum_n e^{-2\frac{(x-x_m)^2+(y-y_n)^2}{\omega_0^2}}, \qquad (5)$$

where $(x_m, y_n) = (x+ms, y+ns)$. The scanning parameter N_{OS} can be estimated by reducing N_P by the accumulation.

Focusing on the accumulation of Gaussian distribution only, in Figure 1 insert (a), (b) and (c), the accumulation is shown for (a) $\varphi = 0$, (b) $\varphi = 0.5$ and (c) $\varphi = 0.9$. At $\varphi = 0$ the difference from peak to valley *(PV)*, is approximately equal to the accumulated peak *(AP)*. Increasing φ to 0.5, leads to a decreased *PV* but increased *AP*. Further increasing φ up to 0.9 increases *AP* drastically, resulting in nearly neglectable *PV*. With increasing φ, *PV* is decreasing and *AP* is increasing.

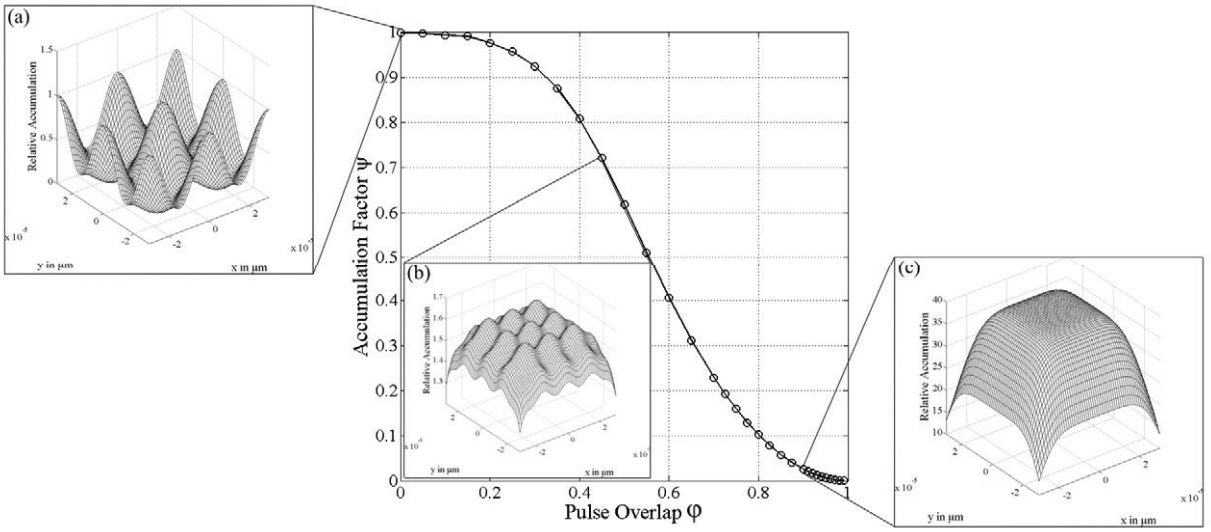

Figure 1. Relation between accumulation factor ψ and pulse overlap φ (Insert left $\varphi = 0$, centre $\varphi = 0.5$ and right $\varphi = 0.9$)

Inverting the peak accumulation, yields a factor $\psi = 1/AP$, which can be used to calculate $N_{OS} = N_P \psi$. If $\varphi = 0.9$ would result in homogenously area of LIPSS, the relative accumulation factor is $\psi = 0.0256$. The static parameter can be converted into dynamic by keeping $\Phi_{LIPSS}(N_P)$ and converting $N_P = 2000$ into $\varphi = 0.9$ and $N_{OS} = 51.2$.

3. Experimental

In our experiment, a commercial, Yb:YAG laser system (Trumpf, Tru Micro 5050), providing pulses with a fixed duration of $\tau = 6.7$ *ps*, wavelength of $\lambda = 1030$ *nm*, and linear polarization, was used. The system delivers pulse energies E_P up to *125 µJ* at a maximum $f_R = 400$ *kHz*. The beam quality factor is $M^2 = 1.15$, determined with a camera based beam diagnostic system (Primes, MicroSpotMonitor). Optionally, the energy of the laser beam can be attenuated externally, using a combination of a zero order wave plate (Thorlabs, WPH10M-1064) and a polarizing beam splitting cube (Thorlabs, PBS 103/203). The average power was measured with a power meter (Coherent, Field Max II-TO) equipped with a thermophile sensor (Coherent, PM 10). Beam manipulation, to position the laser beam on the specimen, was accomplished by a Galvanometer-scanner system (Scanlab, IntelliScan 14). The beam was focused perpendicular to the sample surface by a telecentric f-theta lens (Sill Optics, S4 LFT 0080/126) of $f = 80$ *mm* focal length. All laser experiments were done in air and at atmospheric pressure.

Inspection of specimen surface and measurement of structure geometry were done by optical microscopy (OM,

Leitz, DMRX) equipped with a camera (Leica, DFC 450 CCD), confocal laser scanning microscopy (CLSM, Keyence, VK 9710K) and atomic force microscopy (AFM, Nanosurf, Easyscan 2). The illumination in the CLSM is accomplished by a laser of 408 nm wavelength. Morphologies observed in this paper were named after their appearance in CLSM. The AFM was used in contact mode with a silicon probe (APPNANO, ACL-A).

As specimen, a flat single crystalline silicon mirror substrate (Melles Griot, PM-1025-Si) was used. The mechanically polished surface has a roughness, determined with CLSM, of about Ra 12 nm and Rt 80 nm according to ISO 4287:1997. The hardness, measured with a hardness meter (Shimadzu, DUH-200), was 5.3 GPa or 506 Hv, using a Berkovich indenter at 200 mN load, the elastic modulus was 124 GPa. Cleaning of the specimen was done before and after laser machining using aa Ultra-sonic-bath, filled with Isopropanol.

Friction was measured using a tribometer (CSM, Nanotribometer) with a linear reciprocating module in a ball-on-flat configuration. Normal loads, between $F_N = 2\ mN$ and $F_N = 25\ mN$, were varied. To record stable signals, the number of cycles was 10 and measurement signals were averaged across the number of cycles of 0.3 µm amplitude. The measurement was repeated 4 times, each repetition in a new track on the surface. A single crystalline silicon ball (ISP Optics, Si-B-5) of 5 mm diameter was glued on a bending element, a double leaf spring made of photo structured glass. The roughness of the ball was specified to be below Ra 1 nm. The displacement of the bending element is measured with a fibre optic sensor system, based on reflection intensity variation. The tribological tests were performed at a speed of 0.1 mm/s, orthogonal to the structure orientation and ambient conditions of temperature 20.5 °C and 20% relative humidity in air.

4. Results

4.1. Static experiments

In the first D^2-Experiment the specimen surface was irradiated with single laser pulses of different pulse energy ranging from 0.15 µJ to 125 µJ. Knowing f_R, the pulse energy was determined by measuring the average power. OM and CLSM analysis, of the irradiated surface regions, reveals that the applied pulses damage the material. Each damaged area has different appearance, depending on E_P. Different physical mechanisms contribute, resulting in different types of morphologies.

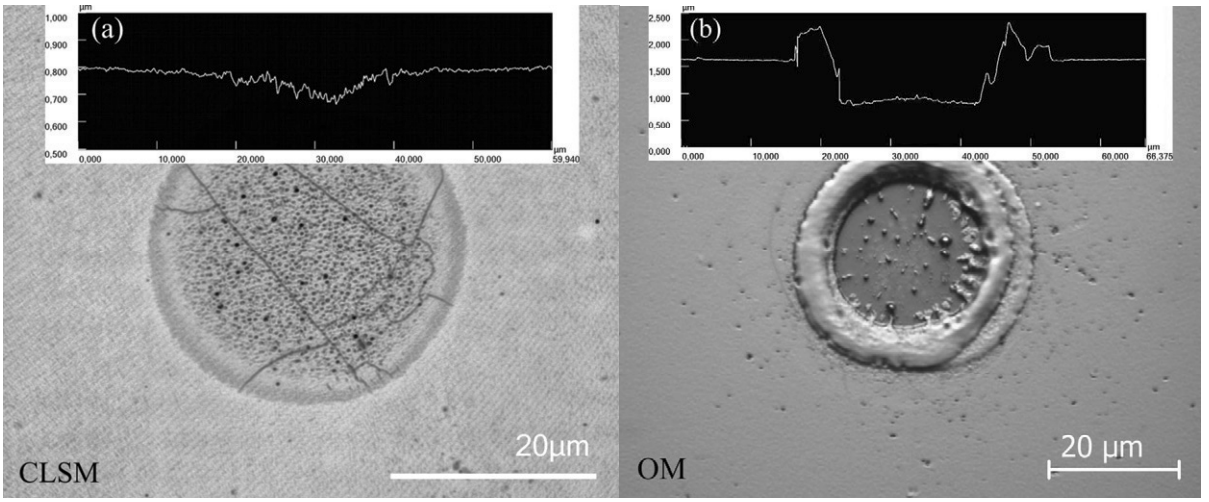

Figure 2. (left) CLSM intensity images $E_P = 1.7\ \mu J$ Insert (a) CLSM height profile (cross-section); (right) OM image $E_P = 33.2\ \mu J$ (oblique illumination and, grey filter, inverted to CLSM) Insert (b) CLSM height profile (cross-section)

Figure 2 (left) shows a CLSM intensity image of an area modified by a pulse of $E_P = 1.7\ \mu J$. At $E_P = 0.26\ \mu J$ the irradiated area appears to be darker then the surrounding material. Further increasing E_P leads to increase in diameter and other type of morphologies. The dark damage is followed by a bright ring. Inside the bright ring an

area with small crater or bubbles, reminiscent of a boiled material can be observed. The CLSM height profile (insert (a) in Figure 2 left) shows an ablation crater in the centre of the boiled area. The irradiated area shows lines which are surface cracks, due to ultra sonic bath cleaning. At $E_P = 4.3\ \mu J$ a rim is formed at the edge of the crater. The rim becomes more protuberant with increasing E_P. At $E_P = 19.1\ \mu J$ a flat, smooth disk in the centre can be observed. With increasing energy, less material remains on the disk. In Figure 2 (right), remaining material at the border and spherical formations on the flat disk can be observed. From $E_P = 50\ \mu J$ upwards material is nearly fully removed from the disk and the rim is surrounded by material splashes, which appears as frozen droplets from a molten phase. The diameter of the flat inner disk increase until $E_P = 125\ \mu J$.

The fluence threshold Φ_{th} of each observed morphology was determined, by measuring D_O and depict D^2 on a semilogarithmic scale as a function of E_P. The minimum energy density, required to modify the surface material by one laser pulse, was found to be the threshold of the dark area $\Phi_D = 0.053\ J/cm^2$ and ablation occurs slightly above the rim threshold of $\Phi_R = 0.537\ J/cm^2$. The beam radius was determined with $\omega_0 = 14.46\ \mu m \pm 0.04$.

Within the single pulse experiment LIPSS were not observed. In the second D^2-Experiment the surface was irradiated with multiple pulses $N_P = 3$ - 200 at 40 Hz and based on the fluence range from the first experiment with single pulses. In order to determine the incubation factor, the Φ_{th} of the dark morphology was determined for every value of N_P. The thresholds decrease with increased N_P. The dependence of $\Phi(N_P) * N_P$ is double logarithmically plotted versus N_P. A fit is applied, which reveals $\xi = 0.91$, compare Figure 3.

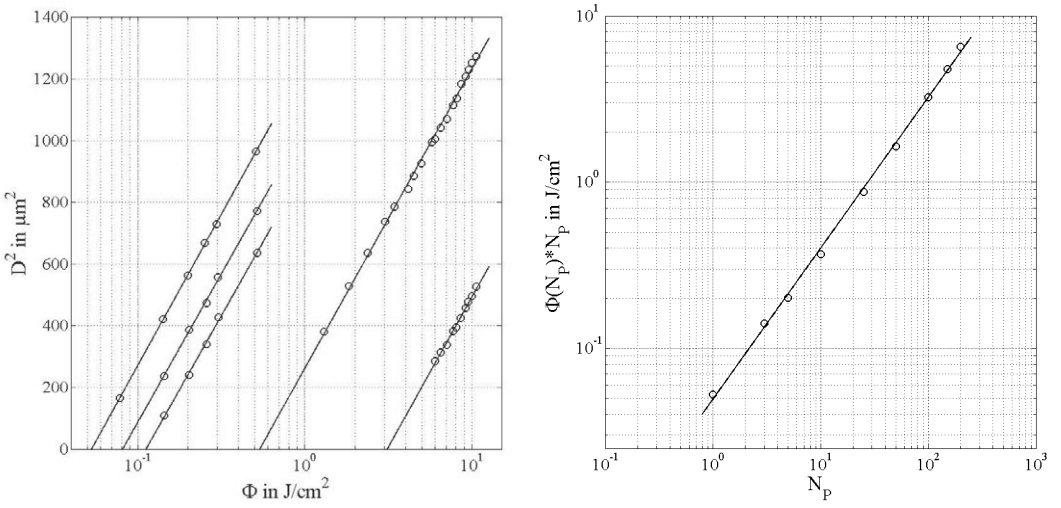

Figure 3. (left) Single pulse thresholds of dark $\Phi_D = 0.053\ J/cm^2$, bright $\Phi_{Br} = 0.081\ J/cm^2$, boiled $\Phi_{Bo} = 0.112\ J/cm^2$, rim $\Phi_R = 0.537\ J/cm^2$ and disk $\Phi_{Di} = 3.112\ J/cm^2$ morphologies; (right) Threshold fluence Φ_D versus N_P

Different types of LIPSS have been observed, type I at $E_P = 0.665\ \mu J$, $N_P = 3$ with periodicity of $\Lambda_I = 0.950\ \mu m$ and an orientation orthogonal to the polarization direction and type II at $E_P = 0.665\ \mu J$, $N_P = 25$ with $\Lambda_{II} \approx 1.6\ \mu m$ and an orientation parallel to the polarization direction. In order to obtain homogeneously formed LIPSS, the multi pulse experiment was extended up to $N_P = 3500$. For $E_P = 0.295\ \mu J$ and $N_P = 2000$ type III was found, with $\Lambda_{III} = 0.750\ \mu m$ and an orientation parallel to the polarization. Φ_{LIPSS} of type III were determined with $\Phi_{LIPSS}(2000) = 0.079\ J/cm^2$. This type of LIPSS occur for a range of N_P.

4.2. Dynamic experiments

In order to achieve a small PV, $\varphi = 0.9$ is selected and in order to structure an area, Φ_{LIPSS} is slightly increased to 0.090 J/cm^2. Instead of the threshold value from D_O, the fluence range between D_I and D_O of these LIPSS is used. Since the theory give only an estimation, N_{OS} was investigated between 1 – 300. As can be observed from Figure 4, at $N_{OS} = 25$ partially LIPSS were obtained, at $N_{OS} = 50$ some regions are structured and at $N_{OS} = 100$ the area is

fully structured. Equal to the static multi pulse experiment, structuring can be observed for a range of N_{OS}. Well above $N_{OS} = 200$ the structure transform into a chaotic pattern. The dynamic experiment was done also for $\varphi = 95$ %, where $\psi = 0.0075$ resulting in $N_{OS} = 15$. In the experiment the structuring starts between 10 and 25 N_{OS}.

In order to measure the friction it was necessary to further extend the rippled area up to 3 x 3 mm^2. Among other things surface irregularities and sample-machine-plan misalignment, has to be taken into account. Therefore Φ_{LIPSS} is slightly increased and a high N_{OS} is selected. Regarding machining time, f_R and v were adopted to $\Phi_0 = 0.097$ J/cm^2, $N_{OS} = 200$, $\varphi = 90$ % and $f_R = 100$ kHz. The machining time was 37 minutes for an area of 3 x 3 mm^2.

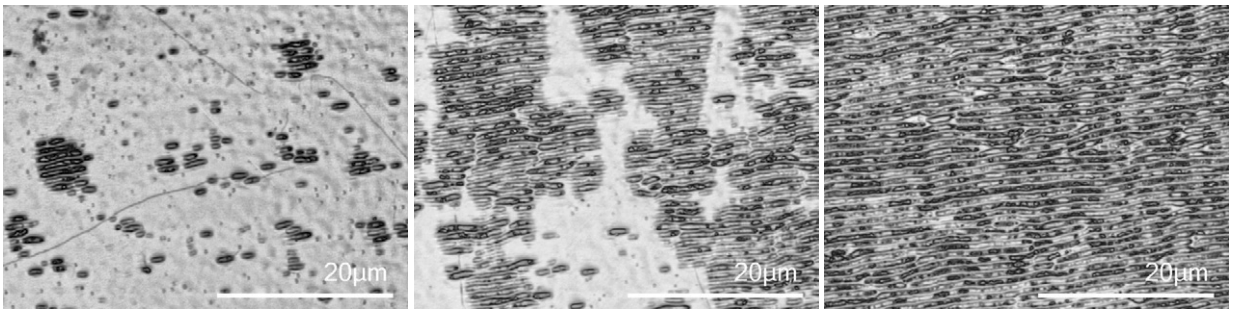

Figure 4. CLSM image of structuring results for $\varphi = 0.9$ and $E_P = 0.295$ µJ (left) $N_{OS} = 25$; (centre) $N_{OS} = 50$; (right) $N_{OS} = 100$

Within the structured area, single laser ablation spots can not be distinguished. The LIPSS obtained type III, show a direction, parallel to the polarization of the laser beam. Orthogonal to this direction, the structure shows an averaged periodicity of $\Lambda_{III} = 750$ nm as found by AFM observations. The amplitude of the LIPSS was found to be 150 nm ± 50 nm in average. The quadratic mean average of profile heights is 50 nm across 10 x 10 µm^2 measurement window.

4.3. Friction measurements

The friction, depending on load, was measured, using a Si ball sliding orthogonal to the structure orientation on the machined as well as on the untreated area. Initial experiments showed that for F_N well over 25 mN LIPSS wear off. As a consequence lower F_N for friction measurements were selected in order to avoid wear and therefore stable and reproducible friction measurements. Below 25 mN, no indication for wear after 10 cycles was found.

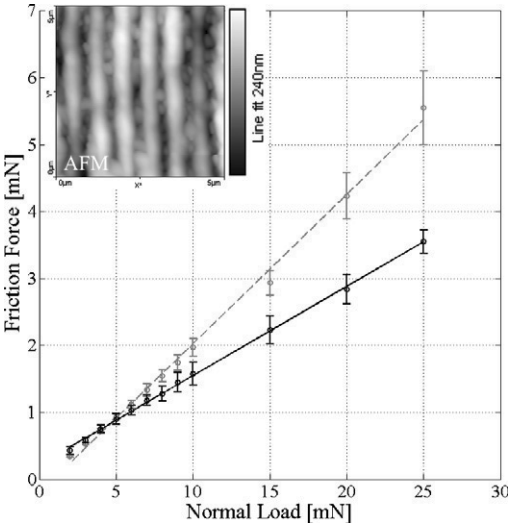

Figure 5. Friction force versus normal load for 2 mN until 25 mN, The dashed line is measured on the structured area and the continuous on the initial surface (Insert: AFM image of the structured area)

According to hertzian equation for point contact, for F_N = 25 mN and Si ball on Si flat, the contact half width is 9 µm, indicating that 24 LIPSS periods are in contact with the ball. The ball deformation was calculated to be 16 nm at 25 mN.

It was found that, the friction force, for F_N = 25 mN, measured on the structured surface is about 1.6 times higher compared to the friction on the untreated, see Figure 5. For F_N below 25 mN the friction properties of the structured area and the initial area tend to get closer together with decreasing load. Between 25 mN and 5 mN the friction force depends on F_N and shows, to a first approximation, a linear relation. Due to technical limitations for loads below 8 mN, the measurement accuracy decreases and both friction signals can not be unambiguously distinguished.

5. Discussion

In order to determine machining parameter for LIPSS we defined two D^2-Experiments. The concept of the first experiment is, to isolate a range of Φ on quantified damage phenomena, given that the laser can damage the material. As estimation for the fluence range we orientated the lower border on the lowest Φ_{th}, which was the dark modified area, and the higher border slightly above Φ_{th} which was close to ablation. In comparison with literature the thresholds are smaller by a factor of 4 to 8 [8, 12], which can be attributed to differences in material properties or methodology. Although the absolute values differ from literature, the identification of a fluence range for the given laser-material combination was possible and in following experiments LIPSS were found within that range. Although the assumption, regarding the fluence range, is based on results from fs experiments [9], this was assumed to be valid for ps pulses as well. The identification is based on Φ_{th} of specific phenomena, such as ablation, and also for ps pulses LIPSS were found to be depend on Φ and N_P [12].

Within this experiment LIPSS were observed for multi pulse irradiation within the isolated fluence range. Although LIPSS are observed for many materials and different laser systems [13-15], there may be a laser-material combination for which LIPSS can not be produced on the surface. It could also be that a special type of LIPSS, occurring above the ablation threshold, will not be observed. In the latter case the fluence range needs to be adjusted.

We observed $\xi = 0.91$ meaning the thresholds we have determined decrease for multiple pulses. Compared to literature value for fs laser irradiation where $\xi = 0.84$ [9] has been found, the incubation of the material used in this experiment is lower. In combination with the incubation law, the Φ_{LIPSS} could give different combinations of Φ and N_P. But experiments show that the periodicity is changing with N_P [10].

We used the accumulation of fluence to convert between static and dynamic results. We investigated the influence of N_P experimentally. Unexpectedly, a sharp transition between partially and fully structured areas was observed. At $\varphi = 0.9$ the PV is sufficient small to cover an area homogenously with LIPSS. The selection of the φ was rather based on experience than on theory. That could be improved by determination of D_I and D_O and consequently the precise fluence range of one type of LIPSS. This fluence range could give an indication for the PV tolerance.

Areas machined within this study were homogenously structured and laser ablation spots can not be distinguished anymore. The detailed analysis by AFM of areas machined with N_{OS} well above 200 shows, this pattern starts to get irregular, which can be detected by small irregularities in the valleys of the structures. This can be due to the high N_{OS} or increased Φ compared to the static experiments. In literature it was observed that if the scanning direction is parallel to the orientation of LIPSS, LIPSS of subsequent spots are interrupted [16]. Another influence on the homogeneity could be due to the dielectric coated mirrors, which could change the polarization for different deflection of the scanning mirror. Both effects were also not observed within this experiment.

The conversion from static parameter to dynamic offers optimization potential. The incubation law could be used to reduce N_P by adjusting Φ and the new N_P could be converted into N_{OS}. The opportunity is given to interchange parameter in a controlled manner. But the static-dynamic conversion is based on two assumptions: 1) For the occurrence of LIPSS the accumulated fluence is the responsible factor. 2) Despite different fluences, due to scanning, the resulting LIPSS are the same. These two assumptions are closely interconnected. Within the transition between static to dynamic, we increase the real N drastically. To what extend N can be exchanged and the influence of subsequent different Φ on physical modifications is not investigated yet. Another point is that we change from static to dynamic the time between pulses from 25 ms to 10 µs. In our results the structures appears to be the same, but using f_R in MHz regime may not give the same result between static and dynamic. If in the static experiment

relaxation time is given and within the dynamic machining that time is drastically reduced, the resulting morphology could be different.

Within this paper three type of LIPSS were observed, type I with $\Lambda_I = 0.950\ \mu m$ and an orientation orthogonal to the polarization direction, type II with $\Lambda_{II} = 1.6\ \mu m$ and an orientation parallel and the ones finally applied type III with $\Lambda_{III} = 0.750\ \mu m$ parallel to the polarization. In literature it is commonly accepted to distinguish Low Spatial Frequency LIPSS (LSFL), which are often found to be orthogonal to the laser polarization and with periodicity in the order of the laser wavelength, and High Spatial Frequency LIPSS (HSFL), with significant smaller periodicity [17]. Fs laser pulse experiments reveal for LSFL on silicon a periodicity of $0.62\ \lambda < \Lambda < \lambda$ [10]. Regarding the periodicity type I and III could be attributed to LSFL, but the orientation of type III is found to be parallel instead of orthogonal to the polarization direction. It is reported that for high number of laser pulses per area, more the $N > 100$, grooves can occur, which can have an orientation parallel to the laser polarization [10]. The period of grooves is found to be 2-3 times the wavelength, although the periodicity is smaller type II could be attributed to that phenomena. The low fluence and orientation of type III would argue for HSFL, but as mentioned above this is not in agreement with the periodicity. Irrespective of the exact qualification of these LIPSS as HSFL or LSFL, type III was used for further analysis.

Within this study the coefficient of friction on the structured area is about a factor of 1.6 at $F_N = 25$ mN higher compared to the initial surface. In [4] a reduction of friction force for nN loads has been observed and in [6] tested under F_N of 2 N and 10 N as well. Reasons for different results could be due to different measurement conditions, under which the load dependence was not explicitly determined, and different laser systems for structure generation.

A decrease of friction between structured and untreated surface, could be due to the reduction of contact area and hence the adhesion part of friction. The influence of roughness on adhesion, for hard elastic solids, was found within an amplitude of 1-10 nm [18-19]. But the structures have an amplitude of 150 nm in average and the initial surface has a roughness of Ra 12 nm. For both surfaces the adhesion should be reduced and a reduction of friction, from structured to initial, should not be due to adhesion.

The increase of friction between structured and untreated surface, could be either due to a modification of topographical or mechanical surface properties. Both surfaces exhibit a certain roughness, the structured surface can be described more accurately by a wavy surface whereas the untreated surface exhibit more stochastically distributed roughness peaks, which could be described by an exponential distribution of asperity heights. The real contact area for the wavy surface scale differently [20] with increasing load then the stochastic rough surface [21]. This may result in a increased friction signal on the wavy surface. Another argument for the influence due to topography could be given by contact mechanical simulations. At $F_N = 25$ mN 24 periods are in contact and the ball deformation is 16 nm. Even if both surfaces deform 50 nm in summation, an inhomogeneous contact is given and may give different friction results.

On the other hand the initial crystalline state of the material could be changed. An indication is given by the irradiation images, which appears to be thermally modified. Further evidence is given by initial experiments with F_N well above 50 mN, where LIPSS starts to erase. For that range of F_N the friction signal of the structured area was further increasing compared to the initial. But wear track analysis show that LIPSS were erased. From that experiment it can not unambiguously distinguished between the influence of topography and material property on the increase of friction.

For loads below 25 mN the friction properties of the structured and the initial area tend to get closer together with decreasing load. The continuation of measurements for smaller geometries in combination with lower loads would be interesting, especially if a cross-over point between high and low friction would be observed. Due to technical limitations, the measurement accuracy decreases at low F_N and could not be improved by repetition of the experiments. Conclusions from that part of the graph, especially for the cross-over point, can not be drawn.

The increase of friction dependent on load could be applicable for areas where accurate clamping is required. Maybe it is possible to optimize the design in the direction, that both, increase and decrease of friction are possible with different normal loads. But the improvement of structure design needs to overcome the limitations by tribological characterization techniques. The relevance for the application also dependence on the long term wear behavior of the structures.

6. Conclusion

Based on the existing knowledge about LIPSS, it was possible to systematically determine parameter for LIPSS. Within this experiment the accumulation of fluence was used to relate parameters obtained in static experiments to parameter for extended area machining. Further investigations are necessary to evaluate the limitations of this new approach. The influence of laser surface texturing on friction was found in the increase of the friction coefficient for structured areas. It was not possible to determine whether this increase is due to the geometry or due to the material properties of the machined area.

Acknowledgements

The author would like to thank Erik de Vries (University of Twente (UT)) for technical support, Dr. Matthijn de Rooij (UT) for evaluation of tribological results, Laura Vargas (UT) for taking SEM images and Dr. Jörn Bonse (Federal Institute for Materials Research and Testing (BAM)) for critical comments on the text of this paper.

References

[1] Stauch, H., et al., Impact of chuck flatness on wafer distortion and stepper overlay - comparison of experimental and FEM-results. Microelectronic Engineering, 1994. 23(1-4): p. 197-201.
[2] Bolle, M. and S. Lazare, Large scale excimer laser production of submicron periodic structures on polymer surfaces. Applied Surface Science, 1993. 69(1-4): p. 31-37.
[3] Yu, J.J. and Y.F. Lu, Laser-induced ripple structures on Ni-P substrates. Applied Surface Science, 1999. 148(3-4): p. 248-252.
[4] Mizuno, A., et al., Friction Properties of the DLC Film with Periodic Structures in Nano-scale. Tribology Online, 2006. 1(2): p. 44-48.
[5] Huang, M., et al., Large area uniform nanostructures fabricated by direct femtosecond laser ablation. Opt. Express, 2008. 16(23): p. 19354-19365.
[6] Yasumaru, N., K. Miyazaki, and J. Kiuchi, Control of tribological properties of diamond-like carbon films with femtosecond-laser-induced nanostructuring. Applied Surface Science, 2008. 254(8): p. 2364-2368.
[7] Das, S.K. and et al., Extended-area nanostructuring of TiO 2 with femtosecond laser pulses at 400 nm using a line focus. Nanotechnology, 2010. 21(15): p. 155302.
[8] Liu, J.M., Simple technique for measurements of pulsed Gaussian-beam spot sizes. Opt. Lett., 1982. 7(5): p. 196-198.
[9] Bonse, J., et al., Femtosecond laser ablation of silicon–modification thresholds and morphology. Applied Physics A: Materials Science and Processing, 2002. 74(1): p. 19-25.
[10] Bonse, J. and J. Krüger, Pulse number dependence of laser-induced periodic surface structures for femtosecond laser irradiation of silicon. Journal of Applied Physics, 2010. 108(3): p. 034903-5.
[11] Jee, Y., M.F. Becker, and R.M. Walser, Laser-induced damage on single-crystal metal surfaces. J. Opt. Soc. Am. B, 1988. 5(3): p. 648-659.
[12] Smirl, A.L., et al., Structural changes produced in silicon by intense 1-μm ps pulses. Journal of Applied Physics, 1986. 60(3): p. 1169-1182.
[13] Siegman, A. and P. Fauchet, Stimulated Wood's anomalies on laser-illuminated surfaces. Quantum Electronics, IEEE Journal of, 1986. 22(8): p. 1384-1403.
[14] van Driel, H.M., J.E. Sipe, and J.F. Young, Laser-Induced Periodic Surface Structure on Solids: A Universal Phenomenon. Physical Review Letters, 1982. 49(26): p. 1955.
[15] Wagner, R. and J. Gottmann, Sub-wavelength ripple formation on various materials induced by tightly focused femtosecond laser radiation. Journal of Physics: Conference Series, 2007. 59(1): p. 333.
[16] Fauchet, P.M. and A.E. Siegman, Surface ripples on silicon and gallium arsenide under picosecond laser illumination. Applied Physics Letters, 1982. 40(9): p. 824-826.
[17] Bonse, J., A. Rosenfeld, and J. Krüger, On the role of surface plasmon polaritons in the formation of laser-induced periodic surface structures upon irradiation of silicon by femtosecond-laser pulses. Journal of Applied Physics, 2009. 106(10): p. 104910-5.
[18] van Zwol, P.J., G. Palasantzas, and J.T.M. De Hosson, Influence of random roughness on the adhesion between metal surfaces due to capillary condensation. Applied Physics Letters, 2007. 91(10): p. 101905-3.
[19] Fuller, K.N.G. and D. Tabor, The Effect of Surface Roughness on the Adhesion of Elastic Solids. Proceedings of the Royal Society of London. Series A, Mathematical and Physical Sciences, 1975. 345(1642): p. 327-342.
[20] Westergaard, H.M., Bearing Pressures and Cracks. Journal of applied Mechanics, 1939. 6: p. 49-53.
[21] Greenwood, J.A. and J.B.P. Williamson, Contact of Nominally Flat Surfaces. Proceedings of the Royal Society of London. Series A, Mathematical and Physical Sciences, 1966. 295(1442): p. 300-319.